LA-UR- 08-5368

Approved for public release; distribution is unlimited.

Title:	Co-operativity among defect sites in AnO2+x and An4O9 (An=U, Np or Pu)
Author(s):	D. A. Andersson, J. Lezama, B. P. Uberuaga and S. D. Conradson
Intended for:	Publication in Physical Review B

Form 836 (7/06)

Co-operativity among defect sites in AnO_{2+x} and An_4O_9 (An = U, Np or Pu)

D. A. Andersson,[1] J. Lezama,[1] B. P. Uberuaga,[1] and S. D. Conradson[1]

[1] *Materials Science and Technology Division, Los Alamos National Laboratory, Los Alamos, NM 87545*

Actinide dioxides derived from the AnO_2 fluorite lattice are of high technological relevance due to their application in nuclear reactor fuels. Oxidation of AnO_2 compounds emerges as a central theme in fuel fabrication, reactor operation, long-term storage forms for both spent fuels and surplus weapons materials, and environmental actinide migration. In this paper we use density functional theory calculations to study the oxidation of uranium, neptunium and plutonium dioxides, AnO_2 (An = U, Np or Pu), in O_2 and O_2/H_2O environments. We pay particular attention to the formation of oxygen clusters (co-operativity) in AnO_{2+x} and how this phenomenon governs oxidation thermodynamics and the development of ordered An_4O_9 compounds. The so-called split di-interstitial, which is composed of two nearest neighbor octahedral oxygen interstitials that are distorted in such a way that they dislocate one regular fluorite lattice oxygen ion to form a cluster of triangular geometry, is predicted to be the fundamental building block of the most stable cluster configurations. We also identify how the formation of oxygen defect clusters and the degree of oxidation in AnO_{2+x} are both governed by the character of the An-5f to excess O-2p charge transfer, i.e. the charge transfer to the O-2p orbitals of the interstitial-like ($+x$) ions, and the ability of the excess O-2p orbitals to hybridize with regular fluorite lattice ions.

I. INTRODUCTION

The technological importance of actinide dioxides, AnO_2 (An = U, Np or Pu), largely originates from their application in nuclear reactor fuels. Today many reactors use UO_2 as the primary fuel component, while low-burnup spent fuels contain large amounts of radioactive materials, in order to reduce the amount of waste requiring long-term storage, there are on-going efforts to develop fast reactors capable of utilizing a larger fraction of the fuel for energy production. This approach calls for complex multi-component fuels that, in addition to the UO_2 matrix, contain significant amounts of transuranic elements (Np, Pu, etc.). Fuel fabrication, reactor operation and long-term storage of waste forms require detailed knowledge of the physics and chemistry of AnO_2 and its oxygen rich/poor forms, $AnO_{2\pm x}$.

The parent fluorite lattice of AnO_2 compounds is relatively simple with An ions occupying every other hole in the cubic oxygen sublattice. However, upon oxidation a range of complex defect configurations are known to form. For example, in addition to the UO_{2+x} solution phase, there are 16 distinct crystallographic phases between UO_2 and UO_3. The properties of AnO_2 demonstrate significant variability along the actinide series, e.g. while UO_2 easily reacts with oxygen[2–4], PuO_2 and later actinide oxides are less prone to oxidation[2,5,6]. PuO_2 seems to require special conditions in order to accomodate excess oxygen[5,7–9]. These complexities are all related to the unique behavior of the An-5f electrons and the unusually high degree of covalent mixing/hybridization in chemical bonds between oxygen and actinides. The structural changes associated with oxidation of AnO_2, as well as the kinetic properties, are important determinants for the microstructural evolution of AnO_{2+x}. The chemical reactivity of AnO_2 and AnO_{2+x} is a key aspect in assessing the environmental hazards of nuclear waste.

UO_2 oxidizes spontaneously in contact with air[2–4] and retains the parent fluorite structure up to the terminal U_4O_9 compound, which exhibits an ordered arrangement of interstitial-like oxygen ions within the fluorite lattice[10,11]. PuO_2 was long thought to be the highest stable oxide of plutonium,[2,6] however Haschke *et al.* found that PuO_2 reacts with moist air to form PuO_{2+x} with $x \leq 0.27$[7,8]. Subsequent EXAFS studies by Conradson *et al.* demonstrated that PuO_{2+x} compounds are more accurately represented as $PuO_{2+x-2y}(OH)_y{\cdot}z(H_2O)$ due to the affinity to H_2O and/or OH^- species[12,13]. No ordered Pu_4O_9 compound has been identified[8]. The realization of hyperstoichiometric PuO_2 raised fundamental questions regarding, e.g., the validity of thermodynamic predictions of PuO_2 solubility and migration from a nuclear waste repository environment. NpO_{2+x} compounds that are related to the NpO_2 fluorite lattice have not been reported in the literature and the experimental phase diagram points to a two-phase-field that involves NpO_2 and Np_2O_5 below $\approx$ 700 K[14,15]. Even though the NpO_{2+x} fluorite phase is meta-stable with respect to NpO_2+Np_2O_5[14,15] or NpO_2+O_2[5,14,15], its properties are important for multi-component (U,Np,Pu,..)O_{2+x} materials since the hyperstoichiometric fluorite phase should be stabilized in uranium containing solid solutions, (U,Np)O_{2+x}.

Theoretical studies of actinide dioxides predict oxidation of UO_2 to be exothermic[16–21] while oxidation of PuO_2 is predicted to be endothermic[17,22,23]. These studies are complicated by the strongly correlated nature of An-5f electrons, which for example cause conventional exchange-correlation functionals, e.g. the local density approximation (LDA), to describe actinide dioxides as ferromagnetic metals instead anti-ferromagnetic Mott insulators. There are, however, promising approaches to address this issue, such as the LDA+U method[19–21,24–27], hybrid density functionals[22,28–30], the self-interaction corrected methodology (SIC)[23] and dy-

namical mean free theory (DMFT)[31]. In addition to the delicate electronic properties of AnO_{2+x}, the interstitial-like excess oxygen ions exhibit complex structural properties that include cluster formation (co-operativity) and strong interaction with the host fluorite lattice[10–13,32–35]. Existing theoretical studies all rely on simplistic structure models of AnO_{2+x} and/or An_4O_9 that essentially ignore clustering effects[16–23].

The present paper is motivated by the persisting incomplete experimental and theoretical understanding of actinide dioxides, in particular for issues regarding oxygen clustering phenomena in AnO_{2+x} and their relation to thermodynamic and kinetic properties. In this paper we investigate the oxidation of UO_2, NpO_2 and PuO_2 by applying density functional theory (DFT) calculations to study the structure, thermodynamic stability and electronic characteristics of interstitial oxygen clusters in AnO_{2+x} and how these clusters may order in the terminal An_4O_9 compounds. The role of H_2O and hydrolysis products (OH^-) in the oxidation process is also addressed. Knowledge of the AnO_{2+x} and An_4O_9 end-member compounds is the first step in understanding the multi-component materials to be used in advanced nuclear fuels.

Our paper is organized as follows. Sec. II describes details of the theoretical methodology to be used. After this, Sec. III A provides a brief overview of existing structure models for the UO_{2+x} system and explains the fundamental aspects of their electronic structure. Sec. III B presents new concepts and results for the geometry and stability of defect clusters in AnO_{2+x}. The corresponding ordering patterns in the terminal An_4O_9 compounds are explored in Sec. III C. We also analyze the particular features of the An-5f electronic structure that drive clustering (co-operativity) in AnO_{2+x}/An_4O_9 compounds and formulate a common framework for UO_{2+x}, NpO_{2-x} and PuO_{2+x}.

II. METHODOLOGY

The DFT calculations were performed with the Vienna Ab Initio Simulation Package (VASP)[36–38] using the projector augmented wave (PAW) method.[39,40] The rotationally invariant LDA+U functional due to Lichtenstein *et al.*[41] was employed to describe the exchange and correlation effects. This method applies the local density approximation (LDA) together with an Hubbard U term that improves handling of the intraband Coulomb repulsion among the 5f electrons. Unlike conventional LDA or GGA, the LDA+U functional captures the Mott insulating properties of the strongly correlated U-5f, Np-5f and Pu-5f electrons in AnO_2 adequately. The LDA+U approach contains two *a priori* unknown parameters; the spherically averaged screened Coulomb energy, U, and the exchange energy, J. For UO_2, U and J parameters of 4.5 eV and 0.51 eV, respectively, were originally derived by Dudarev *et al.*[24] and have since been widely applied[19–21]. Here we adopt these parameters, however in Sec. III C we discuss issues regarding the ability of this parameter set to predict oxidation thermodynamics with high accuracy. We applied $U = 4.0$ eV and $J = 0.7$ eV for the Pu-5f orbitals, which is within the parameter range specified in Refs. 25,26. The U and J parameters for the Np-5f orbitals were set to 4.25 eV and 0.6 eV, which represent an average between the U-5f and Pu-5f values. This choice accounts rather accurately for the experimental lattice parameter and bulk modulus of NpO_2 (see Table I). The occupied Np-5f orbitals are predicted to form a narrow band right at the top of the valence O-2p band, which is similar to the band structure obtained from parameter-free hybrid functionals[28], though the latter predicts a tiny gap between the O-2p band and the Np-5f peak. Spin-polarization was applied for all AnO_{2+x} compounds and, unless otherwise stated, antiferromagnetic spin alignment was used for all compounds. This configuration was obtained as the ground-state for UO_2 and PuO_2, while NpO_2 preferred ferromagnetic ordering by 0.004 eV. Since the ferromagnetic and anti-ferromagnetic NpO_2 structures are almost degenerate, we do not expect the detailed magnetic structure to significantly influence any of the present conclusions. Spin-orbit coupling was not considered, since, even though spin-orbit coupling will change the details of the magnetic ground-state by splitting the f orbitals, this effect is believed to have limited influence on the thermodynamic and structural properties of current interest[30]. The LDA+U lattice constant and bulk modulus predictions for the AnO_2 compounds are summarized in Table I, together with experimental estimates. The calculated lattice parameters agree well with experiments and, even though there are some discrepancies for the bulk modulus, the calculated values are considered to be reasonable, particularly in view of known uncertainties for the experimental PuO_2 bulk modulus[25].

	UO_2	NpO_2	PuO_2
a_0(Å)	5.448 (5.47[57])	5.398 (5.43[57])	5.354 (5.394[7])
B_0(GPa)	218 (207[58,59])	228 (200[58,59])	226 (178[59])

TABLE I: Calculated lattice parameters (a_0) and bulk moduli (B_0) of AnO_2 (An = U, Np or Pu) compounds. Experimental reference values are shown within parenthesis.

A 2×2×2 supercell expansion of the cubic fluorite unit cell was used to study defect properties. The volume of the supercell was fixed at the calculated volume of UO_2, NpO_2 and PuO_2, respectively. All defect calculations used a 2 × 2 × 2 Monkhorst-Pack k-point mesh[42] with a Gaussian smearing of 0.05 eV. The plane-wave cut-off was set to 400 eV. All internal structural parameters were relaxed until the total energy and the Hellmann-Feynman forces on each ion were converged for our purpose (< 0.02 eV/Å). As discussed in Sec. III C, two ordered An_4O_9 compounds have been studied. The unit cells of these structures are spanned by two different sets of vectors; [1

1 0],[0 1 1],[1 0 1] and [2 2 0],[0 0 1],[0.5 -0.5 0], which are defined with respect to the conventional cubic fluorite unit cell. Both of these unit cells contain 26 ions at the An_4O_9 composition. For the first cell we applied a $2 \times 2 \times 2$ Monkhorst-Pack k-point mesh and for the second cell we applied a $2 \times 4 \times 6$ mesh. Volume relaxation was taken into account for both cells. In order to assess the oxidation thermodynamics in O_2 and H_2O chemical environments (gaseous form is assumed throughout this work), reference energies for these molecules must be established. These energies were calculated by placing an isolated molecule inside a large supercell and relaxing the geometry. Since DFT within the LDA formulation is known to overestimate the binding energy of many molecules, we have applied correction terms of 1.2 eV and 1.5 eV for O_2 and H_2O molecules (measured per atom), respectively[43,44]. The oxidation energy of AnO_{2+x} is defined as the energy associated with the $\frac{1}{x}AnO_2 + \frac{1}{2}O_2 \rightarrow \frac{1}{x}AnO_{2+x}$ reaction or, when appropriate, the corresponding reaction that includes H_2O. Recall that negative oxidation energies imply spontaneous oxidation and positive numbers are equivalent to instability of the hyperstoichiometric compounds.

Throughout this work we have calculated spin densities and site projected spin densities to identify the effective valence of ions, e.g. in UO_2 each uranium ion has a projected spin-moment of $\approx 2\ \mu_B$ and each oxygen ion $\approx 0\ \mu_B$, which according to Hund's first rule should correspond to U^{4+} and O^{2-}. A Bader charge density analyses of UO_2 reveals that the actual charge transfer between uranium and oxygen ions does not represent the integer numbers that are expected from their formal valence[21], which reflects that these compounds are far from purely ionic, having a significant covalent character[28].

III. RESULTS AND DISCUSSION

A. Existing AnO_{2+x} structure models and analysis of their electronic structure

1. *Uranium dioxide*

The AnO_2 fluorite lattice has large empty octahedral sites that appear to be the natural location for excess oxygen ions. However Willis *et al.* found that in UO_{2+x} such interstitials tend to aggregate into clusters composed of multiple interstitial ions interacting with regular oxygen ions to form complex defect clusters[33–35]. Willis *et al.*[34] initially proposed the so-called 2:2:2 cluster, which is created by displacing two oxygen ions occupying nearest neighbor octahedral interstitial sites towards each other along the [110] vector connecting the two sites, and at the same time pushing the two neighboring lattice oxygen ions away in the respective $\pm$[111] directions that are perpendicular to the [110] vector, thus effectively creating two oxygen vacancies and four interstitials (see for example Fig. 2 in Ref. 35 for details). Bevan *et al.*[10,11] revised the UO_{2+x} structure model and suggested that the excess oxygen ions occupy the cubo-octahedral holes of the fluorite lattice. In this model each defect cluster contains 12 ions, of which four are ascribed as excess oxygen ions and the remaining eight ions are displaced from their fluorite lattice positions (see for example Fig. 2 in Ref. 10 for details). Analysis of $UO_{2.11}$ and $U_{2.13}$ samples by Murray *et al.*[45] showed that the former compound was better fitted with the 2:2:2 model, while the latter compound was better matched with the cubo-octahedral model, which was interpretted as an indication that the defect structure could be a function of composition and, possibly, sample preparation method. EXAFS measurements by Conradson *et al.* have further illustrated the complexity of UO_{2+x} by suggesting a U-O coordination that includes 1.74 Å bonds[32], which are not present in any existing structure models.

Refs. 47,48 used model potentials to investigate the stability of di-interstitial clusters in UO_{2+x} and, in contrast to experiments, they found the 2:2:2 cluster to be metastable, or even unstable. In its place they predicted the stable di-interstitial oxygen cluster to be composed of three oxygen ions arranged in an equiaxed or equilateral triangle that is situated in a {111} plane above an empty regular oxygen site (see Fig. 1). Andersson *et al.* confirmed these conclusions using DFT calculations and they labeled this defect as split di-interstitial, denoted I_2^X[46]. Here the 'I' denotes an interstitial type of defect, the subscript 2 denotes the number of interstitials that are involved and the superscript 'X' denotes their particular geometric configuration. This notation is used throughout this paper to designate different types of excess oxygen defects. The split di-interstitial is created from two nearest neighbor interstitial ions (a and b in Fig. 1) that move towards a common regular oxygen site, dislocating it (c in Fig. 1), thus creating the split di-interstitial and the vacant site that serves as its center of mass (A, B and C in Fig. 1). Ref. 46 showed that in the low-concentration regime the split di-interstitials are essentially degenerate with two isolated interstitials (I_2^S). Undistorted di-interstitials (I_2^0), i.e. two nearest neighbor interstitials without the accompanying dislocation of any regular oxygen ions, are predicted to be higher in energy than split di-interstitials.

Adding oxygen to UO_2 results in charge transfer from the $5f$ orbitals of U^{4+} ions to the $2p$ orbitals of the excess oxygen ions. The high stability of split di-interstitals in UO_{2+x} can be explained by the fact that this structure allows the orbitals occupied by the transferred electrons to hybridize with the uranium orbitals and thus imitate the uranium-oxygen interaction in the ideal fluorite lattice, in particular the covalent contribution to the uranium-oxygen bonding. This process enables the excess O-$2p$ orbitals to move down from the U-$5f$ states at the Fermi level to the main O-$2p$ band, thus decreasing the band energy and, unless the corresponding increase in electrostatic energy among ions dominates, also the total energy (illustrated in Fig. 2). As a consequence,

the O-2p–U-5f gap found in UO_2 (i.e. the gap between the main O-2p and the occupied U-5f states) diminishes or even disappears. Oxygen ions in octahedral interstitial sites are unable to interact as efficiently as split di-interstitials with the uranium ions and, consequently, the excess O-2p orbitals for octahedral interstitials cannot merge with the main O-2p band. For this reason they do not experience the same gain in band energy as split di-interstitials. However, due to the larger separation of O^{2-} and U^{5+}/U^{6+} ions, octahedral interstitials are more favorable from the perspective of Coulomb repulsion among ions. To summarize, the mechanism that drives the formation of oxygen clusters in UO_{2+x} is the ability to decrease the band energy via increased uranium-oxygen orbital hybrydization. These features are even more evident for U_4O_9 compounds than for small clusters of point defects in UO_{2+x}. Fig. 2 illustrates the band structures of two U_4O_9 compounds; one based on octahedral interstitials and another one composed of ordered split di-interstials. We pay particular attention to the highlighted difference in the band structure position of the excess O-2p orbitals between these two structures. Integration of the density of states from $-\infty$ to the Fermi level measures the band energy and the shift of the O-2p states for the split di-interstitial structure yields a lower energy and thus constitutes a stabilizing contribution.

Let us take a closer look at the underlying mechanisms for the hybridization features discussed in the previous paragraph. The projected DOS for UO_2 (partially illustrated in Fig. 3) reveals that there is a sizable U-5f/U-6d contribution in the main O-2p band. At the same time, an electron count shows that all the U-5f electrons that are expected from the formal valence of the U^{4+} ions (two) are located in the U-5f peak above the edge of the main O-2p band. This implies that the U-5f/U-6d contribution in the O-2p band originates from overlap/hybridization of nominally filled O-2p orbitals with nominally empty U-5f/U-6d orbitals (empty means not occupied by electrons expected from the formal valence count). By plotting the charge density that derives from the hybridized main O-2p band (not shown) we can see that the U-5f/U-6d contribution is indeed centered around uranium ions, which accentuates that there is a real contribution from uranium orbitals in the main O-2p band. This hybridization mechanism is also consistent with the fact that Bader charge analysis gives ionic charges that deviate significantly from the nominal charges of U^{4+} and O^{2-} ions[21]. Moreover, since the localized magnetic moments on uranium and oxygen ions correspond to the formal valence occupation of the 5f and 2p bands, the hybridized 5f/6d/2p-states must be occupied by spin-paired electrons to give a net zero contribution to the magnetic moment. This type of hybridization is not available for the octahedral interstitial oxygen ions in U_4O_9(Oct.), since their interaction with the uranium ions is shielded by the cubic cage of regular fluorite oxygen ions. Instead the nearest neighbor uranium interaction for the octahedral oxygen interstitials is such that their O-2p orbitals almost overlap with the U-5f states in the band gap, as indicated by Fig. 2. In fact the integrated number of electrons inside the band gap peak in U_4O_9(Oct.) corresponds to the sum of the number of U-5f electrons expected from the formal valence of $U^{4+}/U^{5+}/U^{6+}$ ions and the number of O-2p electrons that belong to octahedral interstitial ions. The split di-interstitial U_4O_9 structures, on the other hand, allow the O-2p orbitals of both the regular fluorite oxygen ions and the excess ions to overlap/hybridize with the nominally empty U-5f/U-6d orbitals, which, as mentioned above, facilitates for the excess O-2p orbitals to move down from the U-5f states at the Fermi level to the main O-2p band (Fig. 2) and thus decrease the band energy. In agreement with this picture, a plot of the charge density contribution from the upper part of the valence band clearly reveals that there is a major contribution from the octahedral interstitial ions in U_4O_9(Oct.), while the corresponding plot for the split di-interstitial U_4O_9 structures give a more equal contribution from all oxygen ions. We conclude that the overlap of excess O-2p orbitals with the main O-2p band is in fact driven by the hybridization of excess O-2p orbitals with nominally empty U-5f/U-6d orbitals made possible by the particular structural distortion for split di-interstitials. Fig. 2 also reveals that the calculations predict the band gap (valence to conduction band) to decrease by ≈ 0.45 eV for structures built from split di-interstitials, as compared to octahedral interstitials, and by ≈ 0.70 eV compared to UO_2. This is an indicator of the changes in O-2p–U-5f/U-6d hybridization that takes place for split di-interstitial structures. The increased hybridization for the split di-interstital structure leads to smaller O-O distances and also shorter separation of the charge compensating An^{5+} ions, both of which yield a destabilizing contribution mainly due to increased electrostatic (Coulomb) repulsion among ions. Qualitatively, this implies that the defect stability in UO_{2+x} is a competition between hybridization (decrease of the band energy) and Coulomb repulsion among ions. The former favors the split di-interstital type of structures while the latter favors structures based on octahedral interstitals.

2. *Neptunium and Plutonium dioxides*

Band structure calculations reveal that the 5f electrons in UO_2 are situated ≈ 0.6 eV above the O-2p valence band edge, while the corresponding Np-5f states are right at the top of the O-2p band. For PuO_2 the 5f states overlap with the O-2p band and together they form a more or less continuous band. These results are consistent with calculations using the hybrid-DFT method[30]. Due to the shift in position of the occupied 5f orbitals, the gain in band energy coming from charge transfer and hybridization between neptunium ions and the excess oxygen ions should be smaller than for UO_{2+x}. Another way of stating this would be that the difference be-

tween the delocalization energy of Np-5f electrons (Np^{4+} $\rightarrow$ Np^{5+}) and the energy of these electrons occupying the (hybridized) O-2p band decreases compared to UO_2. This effect is even stronger for PuO_{2+x} and, in fact, the Pu^{4+} to excess oxygen charge transfer may result in increasing band energy. Fig. 3 shows the change in band structure between UO_2, NpO_2 and PuO_2. We note that the shift in the separation of the O-2p and An-5f bands is a qualitative measure of the ease of oxidation; large positive separation (arrow pointed to the right in Fig. 3) implies negative oxidation energy and as the An-5f states move down below the main O-2p band edge oxidation becomes more difficult (shorter "left " arrow and arrow pointed to the right in Fig. 3). Qualitatively, upon oxidation the An-5f electrons move to the top of the O-2p band and, consequently, their relative position is closely related to the oxidation thermodynamics, via the band energy. We remark that this picture corresponds to maximum gain in band energy and, as we have seen in Fig. 2, the real band structure for UO_{2+x} is somewhat more complicated but, qualitatively, the concept presented above is still valid. An immediate consequence of this band structure effect is that the excess oxygen ions in PuO_{2+x} exhibits a different valence state than for UO_{2+x}. Analyses of spin densities reveal that excess oxygen ions in UO_{2+x} act as O^{2-}, while the corresponding state for PuO_{2+x} is $O^{(2-\delta)-}$, where $0 < \delta < 0.5$ and the exact δ value is structure dependent. δ values close to 0 correspond to split di-interstitial structures and the higher values to structures based on regular octahedral interstitials, i.e. the higher degree of hybridization for split di-interstitials facilitates higher valence but compared to UO_{2+x} this process is still incomplete. The charge-compensating plutonium ions also deviate from the pentavalent state of U^{5+} ions and exhibit a partially reduced valency. All together this indicates that complete charge transfer between localized Pu-5f and excess O-2p orbitals is not favourable. Here, and also in the remainder of this paper, charge transfer refers to delocalizing one electron from the 5f orbitals and allowing it to participate in An-O bonding, which, as discussed above, includes both charge transfer and hybridization. The valence states in NpO_{2+x} suggest that it should be classified in the same category as PuO_{2+x}, but with smaller δ values, which is consistent with the occupied Np-5f states being situated at the top of the O-2p band and thus in-between the position of the occupied U-5f and Pu-5f orbitals. The fact that charge transfer is incomplete in PuO_{2+x} and NpO_{2+x} creates a hole in the O-2p band, which, from a chemical point of view, is unfavorable and, as discussed in Secs. III C and III D, this has important consequences for the oxidation thermodynamics.

The band structure concepts presented above will be used as basis for the forthcoming discussion of AnO_{2+x}/An_4O_9 structures and their thermodynamic stability.

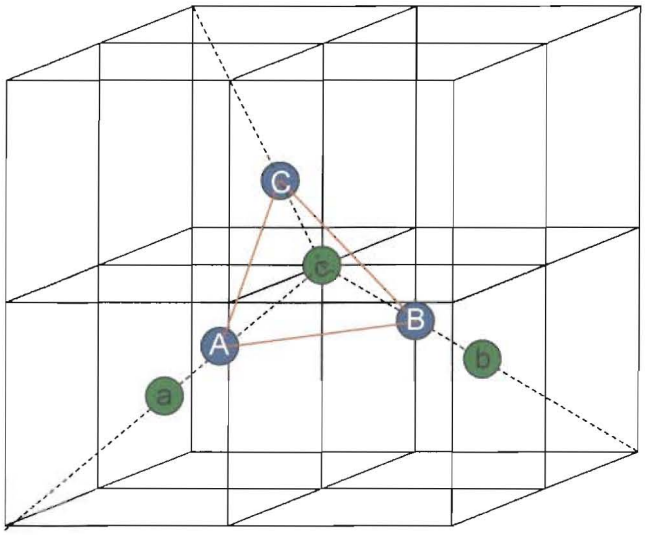

FIG. 1: (Color online) Idealized schematics of the structure of the undistorted (I_2^O, lower case letters) and split (I_2^X, upper case letters) di-interstitial structures. The cubes represent the simple-cubic oxygen sublattice; for clarity, uranium ions are not shown. The I_2^O structure has two oxygen interstitials (a and b) in octahedral interstitial sites in the lattice, while the remaining oxygen atoms remain in more or less perfect lattice sites. The I_2^X structure constitutes an equiaxed/equilateral triangle that is situated on top of an empty regular fluorite lattice oxygen site.

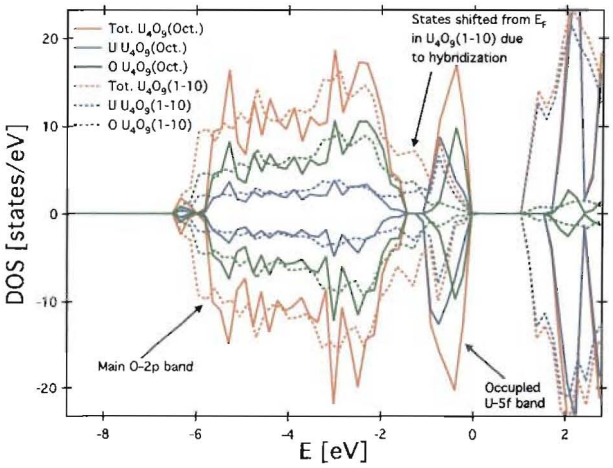

FIG. 2: (Color online) Densitiy of states (DOS) and projected density of states (PDOS) for U_4O_9 constructed from an ordered arrangement of split di-interstitials, U_4O_9(1-10), and octahedral interstitials, U_4O_9(Oct.). Notice that the U-5f–O-2p gap remains for the octahedral interstitial structure, while for the split di-interstitial structure the O-2p states overlapping with U-5f peak in the octahedral structure moves down to overlap with the main O-2p band. There is also a small downward shift of some of the occupied U-5f states. Moreover, the (valence-conduction) band gap decreases by ≈ 0.45 eV for the split di-interstitial structures, as compared to octahedral interstitials. The highest occupied state is at 0 eV.

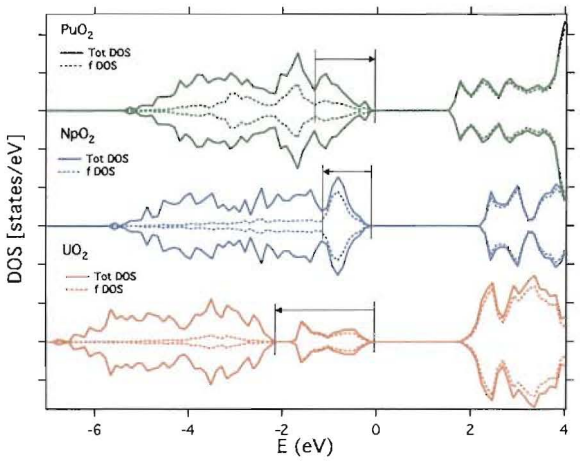

FIG. 3: (Color online) The band structure of UO_2, NpO_2 and PuO_2. The position of the An-5f bands is shown in dashed lines, including both localized states and states that are hybridized with the O-2p band. The arrows indicate the separation of the localized An-5f states and the O-2p bands. In particular for NpO_2 and PuO_2 this measure is qualitative, since the An-5f and O-2p bands exhibit strong hybridization. The highest occupied state is at 0 eV.

B. New geometries and stabilities of oxygen clusters in AnO_{2+x}

1. *Uranium dioxide*

Table II summarizes the oxidation energies (stabilities) of di-interstitial defect clusters in UO_{2+x}, NpO_{2+x} and PuO_{2+x} (for now we focus on di-interstitials, I_2, and ignore other data in Table II). The UO_{2+x} data is partially reproduced from Ref. 46. Comparing the results for NpO_{2+x} and PuO_{2+x} with UO_{2+x}, the main conclusion is that the oxidation energies for NpO_{2+x} and PuO_{2+x} are much less negative and, as a result, NpO_2 and PuO_2 should be more difficult to oxidize. PuO_{2+x} is even predicted to have positive oxidation energy, which implies that PuO_2 should not react with O_2, unless another lower energy reaction path is available (discussed in Secs. III C and III D). The observed UO_2, NpO_2 and PuO_2 sequence of increasing oxidation energies correlates with the change in the position of the An-5f orbitals compared to the O-2p band between UO_2, NpO_2 and PuO_2. The associated decreased gain in O-2p band energy relative to the 5f delocalization energy explains the high oxidation energy for NpO_{2+x} and PuO_{2+x}. The stability of split di-interstitials and regular octahedral interstitials is switched between NpO_{2+x} and UO_{2+x}. This trend is further strengthened for PuO_{2+x}. In all cases, the explicit dislocation of a fluorite oxygen ion in I_2^0 to form I_2^X is accompanied by substantial lowering of the energy, which follows from the increased hybridization of excess O-2p orbitals (gain in band energy) that is facilitated by this structural distortion. For UO_{2+x} the oxidation energy of a single oxygen interstitial in the $2\times2\times2$ supercell (I_1) is lower than for di-interstitial clusters, which means that in the dilute limit the binding energy for any di-interstitial cluster is negative and they should thus dissolve. This energy balance is an effect of the aforementioned competition between Coulomb repulsion among ions and hybridization. In the low oxygen concentration regime the former contribution dominates over the latter.

The cubo-octahedron cluster (I_4^C) proposed for UO_{2+x}[10,11] contains four excess oxygen ions and thus represents a larger and more extended defect than the di-interstitial type of clusters. In order to evaluate its stability we have studied a single cubo-octahedral cluster embedded in the $2\times2\times2$ supercell and, for comparison, we have also studied clusters composed of two split di-interstitials, hereby denoted split quad-interstitial (I_4^X), as well as four octahedral interstitials homogeneously distributed within the $2\times2\times2$ supercell (I_4^S). The geometry of the split quad-interstitial is depicted in Fig. 4 and further discussed below. The stabilities (oxidation energies) of these structures are collected in Table II (labeled as I_4). The split quad-interstitial is the most stable configuration, followed by the cubo-octahedron cluster and both of them are more stable than the structure based on regular octahedral interstitials. The key electronic structure difference between the split quad- and octahedral-interstitial structures is that the former enables efficient O-2p hybridization for the excess ions and thus lowers the band energy, in the same way as for the split di-interstitial structures, while the latter pins the excess O-2p states at the Fermi level and, as a result, does not allow the same lowering of the band energy. We recall that, compared to split di-interstitials, octahedral interstitial structures benefit from lower Coulomb repulsion among ions. However, unlike the split di-interstitial/octahedral interstitial balance in the low-concentration range (I_2^X vs. I_2^S), for the intermediate oxygen concentration range the gain in band energy due to hybridization outweighs the increase in Coulomb repulsion to clearly favor split quad-interstitials over seperated octahedral interstitials (I_4^X vs. I_4^S). The oxidation energy of split quad-interstitials is lower than for split di-interstitials, which means that the split quad-interstitial is a bound state of two split di-interstitials (0.37 eV per split quad-interstitial cluster). The high stability for the split quad-interstitial seems to follow from a combination of further increased hybridization and more efficient handling of the Coulomb contribution. The binding energy of split quad-interstitials with respect to single interstitials in the dilute limit is still negative by a small amount (0.10 eV/split quad-interstitial). This suggests that the split quad-interstitial cluster may break up in the low oxygen concentration regime, but should be stable for intermediate and high oxygen concentrations. The geometry of the most stable split quad-interstitial configuration is such that the two split di-interstitials are aligned along the [0.5 0 0] lattice vector and rotated 180° with respect to each other (see Fig. 4). The cubo-octahedron structure shares some of the electronic structure features with the split quad-interstitials,

	$An_{32}O_{65}(I_1)$	$An_{32}O_{66}(I_2^0)$	$An_{32}O_{66}(I_2^S)$	$An_{32}O_{66}(I_2^X)$	$An_{32}O_{68}(I_4^X)$	$An_{32}O_{68}(I_4^S)$
UO_2	−2.45	−2.13	−2.36	−2.33	−2.42	−2.22
NpO_2	−0.15	0.16	−0.16	−0.17	−0.31	−0.18
PuO_2	0.79	1.07	0.13	0.45	0.07	0.04
	$An_{32}O_{68}(I_4^C)$	An_4O_9(Oct.)	$An_4O_9(111_0)$	$An_4O_9(111)$	An_4O_9(1-10)	An_4O_9(bcc)
UO_2	−2.25	−1.86 [−0.05 Å]	−2.05 [−0.03 Å]	−2.11 [−0.01 Å]	−2.25 [−0.02 Å]	−2.47
NpO_2	N/A	0.39 (−0.37) [0.01 Å]	−0.18 [−0.01 Å]	−0.22 [-0.01 Å]	−0.56 [−0.01 Å]	−0.79
PuO_2	N/A	0.34 (−0.13) [0.03 Å]	0.00 [0.02 Å]	0.13 [0.01 Å]	0.46 [−0.01 Å]	−0.14
	An_4O_9(bccr)	An_4O_9(Cubo)	$AnO_2(H_2O)_{\frac{1}{32}}$	$AnO_2(OH)_{\frac{1}{32}}$	$An_4O_8(OH)_2$	
UO_2	−2.57	−2.13	N/A	−2.22	−1.96 [0.03 Å]	
NpO_2	−0.75	N/A	N/A	−0.70	−0.84 [0.03 Å]	
PuO_2	−0.09	N/A	0.48	−0.06	−0.71 [0.03 Å]	

TABLE II: The oxidation energy for various defects in AnO_{2+x}, differently ordered An_4O_9 compounds and hydrogen-containing AnO_{2+x}/An_4O_9 compounds. The type of defect and defect ordering is indicated within parenthesis, e.g. $An_{32}O_{65}(I_1)$ for one single interstitial in the 2×2×2 supercell. See text for labeling. The values within parenthesis for Pu_4O_9(Oct.) and Np_4O_9(Oct.) correspond to an octahedral interstitial compound that contains O_2 species (see text). All energies are in eV and measured per excess oxygen ion. For the small unit cells, the values within brackets represent the change in lattice parameter (in Å) compared AnO_2 (volume relaxation was not performed for the cases where this number is missing). N/A designates that this particular compound was not studied.

but, as indicated by the higher oxidation energy of the cubo-octahedron structure, these features are not optimized to the same extent for cubo-octahedrons as for split quad-interstitials.

2. *Neptunium and Plutonium dioxides*

According to the I_1 and I_2^X oxidation energies in Table II, for NpO_{2+x} the binding energy of spit di-interstitials is negative and, as for UO_{2+x}, this defect should thus be unstable for small x. For PuO_{2+x} the binding energy is positive, indicating a shift in the balance between hybridization energy and Coulomb repulsion, which stabilizes clusters over isolated interstitials. Table II also contains the stability of split quad-interstitial clusters and separated octahedral interstitials in NpO_{2+x} and PuO_{2+x}. The NpO_{2+x} results confirm the trends for UO_{2+x}, in the sense that the split quad-interstitial is predicted to be the most stable state. For PuO_{2+x} the structures exhibit rather similar energies. Compared to UO_{2+x}, the oxidation energy of split quad-interstitials remain high for both NpO_{2+x} and PuO_{2+x}.

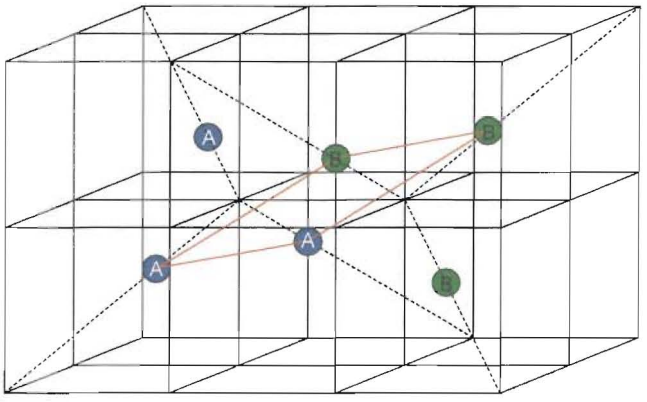

FIG. 4: (Color online) Idealized schematics of the split quad-interstitial (I_4^X). The cubes represent the simple-cubic oxygen sublattice; for clarity, uranium ions are not shown. The dashed lines indicate the particular cube diagonals, along which the interstitial and regular oxygen ions that belong to the defect cluster are displaced. The two split di-interstitials that make up the quad-interstitial are highlighted by A and B, respectively. The parallellogram formed by the adjoining base lines of the two split di-interstitials is outlined.

C. Ordering of oxygen clusters in An_4O_9

1. *Uranium dioxide*

Below 500-1400 K UO_{2+x} phase separates into UO_2 (UO_{2+x}) and ordered U_4O_9 (U_4O_{9-y})[1,10]. The temperature at which the two-phase field transforms into a solid solution is a strong function of composition[1,10]. U_4O_9 is envisioned to be an ordered arrangement of the oxygen defects/clusters in UO_{2+x}. Early neutron diffraction experiments indicated that U_4O_9 should be described within a 4 × 4 × 4 expansion of the conventional fluorite unit cell and Allen *et al.*[49] proposed an ordered arrangement of 2:2:2 clusters along the [1-1 0] lattice vector, or equivalent directions. This model was later rejected due to incompatibilities with neutron diffraction data[10,21]. The most recent U_4O_9 (U_4O_{9-y}) structure model is an intricate arrangement of the cubo-octahedron clusters within the 4 × 4 × 4 unit cell[11].

Proceeding from the ground-state configurations of the

split di- and quad-interstitials, we investigate how these may order at the U_4O_9 composition. Two different ordering patterns of split di-interstitials have been considered; split di-interstitials ordered in every fourth {111} plane (U_4O_9(111)) and split di-interstitials ordered along [1-10] lattice vectors (U_4O_9(1-10)). These structures are spanned by [1 1 0],[0 1 1],[1 0 1] (U_4O_9(111)) and [2 2 0],[0 0 1],[0.5 -0.5 0] (U_4O_9(1-10)) sets of basis vectors. Each unit cell contains 26 atoms and there is one split di-interstitial per unit cell. U_4O_9(111) is a natural extension of the fact that split di-interstitials occupy {111} planes and U_4O_9(1-10) is inspired by the U_4O_9 structure proposed by Allen *et al.*, but instead of the 2:2:2 cluster, the U_4O_9(1-10) structure uses the split di-interstitial as the expansion unit. Viewed along the [111] direction the fluorite lattice is composed of hexagonal U and O layers arranged in a -O-O-U-O-O-U-O-O- sequence. Fig. 5b shows the geometry of the {111} plane containing the split di-interstitials in U_4O_9(111). The split di-interstitial oxygen ions are slightly displaced out of the {111} plane, as compared to the regular fluorite oxygen ions in the same {111} plane. The charge compensating U^{5+} ions fully occupy the next nearest neighbor uranium plane with respect to the split di-interstitials. Ref. 50 discusses how fluorite derived structures can be rationalized in terms of {111} stacking motifs and the U_4O_9(111) structure obviously belongs to this class, though this particular stacking pattern has not been previously identified. Below we outline how all the proposed U_4O_9 structures can in fact be rationalized in terms of {111} stacking motifs based on split di-interstitials.

The starting point for the U_4O_9(1-10) structure is a chain of split di-interstitials separated by [0.5 0 0] and [0 -0.5 0] vectors, which yields a unit cell periodicity of [0.5 -0.5 0]. Upon geometry optimization this structure relaxes significantly and the [0.5 -0.5 0] ordering of triangular split di-interstitial motifs transforms into a new stacking pattern, still along [0.5 -0.5 0], but composed of four interstitial-like oxygen ions arranged in a parallelogram. This parallelogram is created from the split di-interstitial by displacing one additional regular oxygen ion from its lattice site, which may also be interpreted as the two excess oxygen ions dislocating two regular oxygen ions, instead of one for the split di-interstitial. The adjoining split di-interstitials in the split quad-interstitial cluster also creates a parallelogram (see Fig. 4), which is equivalent to the parallelogram in the U_4O_9(1-10) structure. Thus, U_4O_9(1-10) can also be viewed as an interconnected ordering of split quad-interstitials along the [1-10] lattice vector (note that the periodicity is [0.5 -0.5 0]). The U^{5+} ions in the U_4O_9(1-10) structure occupy the four nearest neighbor positions with respect to the defect oxygen parallelogram. Also the U_4O_9(1-10) structure can be visualized within a {111} stacking model, see Fig. 5c. The cluster ions form chains in the {111} planes and, since the excess ions/defects occupy every {111} plane instead of every fourth plane as for U_4O_9(111), the concentration of excess ions/defects in each U_4O_9(1-10) {111} plane is 1/4 of the corresponding U_4O_9(111) {111} concentration. The {111} planes in U_4O_9(1-10) are not stacked directly on top of each other, but instead they are shifted in order to avoid overlap of the defect chains. The (111) stacking sequence involves a periodicity of twelve oxygen planes. Relaxation results in small out of plane shifts within each U_4O_9(1-10) {111} plane.

The split quad-intersitial clusters may also be arranged as separate units within the fluorite lattice and, in principle, arbitrary superstructures can be created by varying the stacking and orientation of these units. This idea is similar to the approach used for construction of an ordered U_4O_9 structure from cubo-octahedral clusters. We have investigated two of the most probable configurations within the $2 \times 2 \times 2$ supercell; in the first case the split quad-interstitials are ordered along the [111] vector (U_4O_9(bcc)) and in the second case, one of these split quad-interstitial units is rotated 90° with respect to the other cluster (U_4O_9(bccr)). Notice that the split quad-interstitials in U_4O_9(bcc) and U_4O_9(bccr) form a bcc lattice, hence the bcc and bccr notation. Even though the true ground-state structure of U_4O_9 may exhibit longer stacking sequence of split quad-interstitials than allowed within the $2 \times 2 \times 2$ cell, we believe that U_4O_9(bcc) and U_4O_9(bccr) serve as appropriate modeling compounds, capable of capturing the relevant physics of the U_4O_9 superstructures. Due to the specific geometry of split quad-interstitials, both U_4O_9(bcc) and U_1O_9(bccr) in fact involve stacking of {111} planes with an ordered arrangement of split di-interstitials. In these two cases the split di-interstitials occupy every oxygen plane and Fig. 5 illustrates the internal geometry for U_4O_9(bcc). The split quad-interstitials are made up of two split di-interstitials overlapping between nearest neighbor {111} planes. For U_4O_9(bcc) the {111} stacking periodicity involves six oxygen planes. The {111} planes in U_4O_9(bccr) exhibit the same type of in-plane pattern of split di-interstitials as U_4O_9(bcc), but the stacking sequence differs between the two structures. There are rather significant out of plane distortions for the split di-interstitials in both U_4O_9(bcc) and U_4O_9(bccr). Following the recipe for U_4O_9(bcc), we have also built U_4O_9 structure models by inserting two cubo-octahedral clusters separated by the [111] vector in the $2\times2\times2$ cell. These structures represent a simplified version of the $4\times4\times4$ cubo-octahedron structure reported by Bevan *et al.*[10]. As reference, we have calculated the stability of U_4O_9 constructed from regular octahedral interstitials (U_4O_9(Oct.)) and undistorted di-interstitials ($U_4O_9(111_0)$). We note that the postulated cubo-octahedron U_4O_9 model was constructed to exhibit $\bar{4}3m$ symmetry, as was derived from neutron diffraction experiments on the intermediate temperature β-U_4O_9 structure[51]. We have intentionally relaxed this requirement for the structures proposed in the present work.

Table II shows that U_4O_9(bccr) is the most stable U_4O_9 compound, followed by U_4O_9(bcc). U_4O_9(1-10) and U_4O_9(111), as well as any structures based on oc-

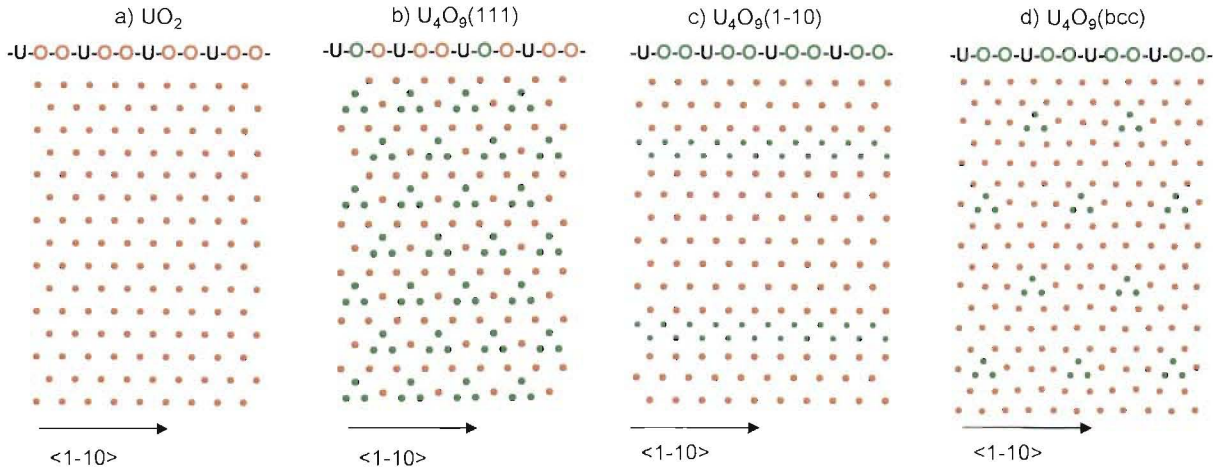

FIG. 5: T (Color online) a) The hexagonal pattern of oxygen ions in a {111} plane of the UO_2 fluorite lattice. b), c) and d) illustrate the ordering of split di-interstitials (green/light) in {111} planes for b) U_4O_9(111), c) U_4O_9(1-10) and d) U_4O_9(bcc). Viewed along the {111} direction, the fluorite lattice is composed of the '-U-O-O-U-O-O-U-O-O-U-O-O-' sequence of uranium and oxygen planes. In a), b), c) and d) the red/dark 'O' character symbolizes a regular oxygen plane and the green/light 'O' character symbolizes an oxygen plane that contains excess oxygen ions/defects. The detailed stacking sequence is further discussed in the text.

tahedral interstitials, are considerably higher in energy. With reference to Fig. 5 and Table II, we emphasize the stabilizing contribution from the covalent bonding (hybridization) in split di-interstitial type of defects and, additionally, the fact that distributing such defects among several planes (compare for example U_4O_9(bcc) and U_4O_9(111)) and maximizing the intra-planar separation of split di-interstitials (compare for example U_4O_9(bcc) and U_4O_9(1-10)) lowers the contribution from Coulomb repulsion among ions. Fig. 6 demonstrates that our calculations predict a UO_2-U_4O_9 two-phase field at low temperature, which is in agreement with experimental findings[1,10]. This two-phase field only emerges when the U_4O_9(bcc) or U_4O_9(bccr) structures are taken into account and this emphasizes the strong influence that clustering/co-operativity has on the UO_{2+x} phase diagram. The most negative UO_{2+x} oxidation energies are obtained for regular octahedral interstitials at low oxygen concentrations (large separation between interstitials and small contribution from Coulomb repulsion) and the U_4O_9(bcc)/U_4O_9(bccr) structures (high degree of hybridization). For low x, minimizing Coulomb repulsion among ions dominates over hybridization (octahedral interstitials, I_2^S, are more stable than split di-interstitials, I_2^X), while, for increasing x, Coulomb repulsion between defects becomes more important and, in order to compensate, hybridization is increased by shifting the defect population towards split di-interstitial type structures. The most efficient way of achieving this balance is to phase separate into UO_2, or UO_{2+x} with low x, and the U_4O_9(bcc)/U_4O_9(bccr) structures, a reaction which simultaneously minimizes Coulomb repulsion and maximizes hybridization. This mechanism is the underlying driving force for the UO_{2+x}-U_4O_9 phase separation observed in experiments. For U_4O_9(111), U_4O_9(bcc)

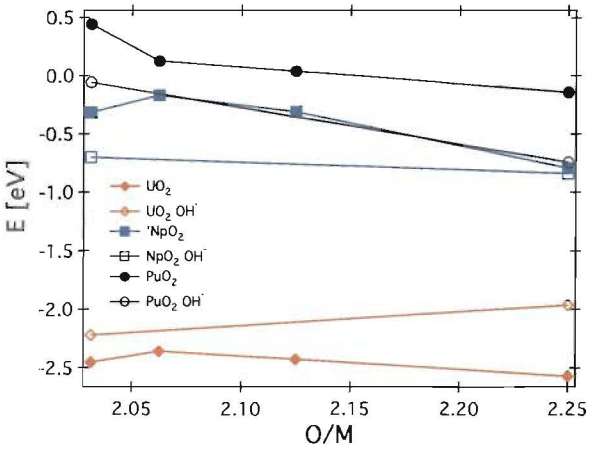

FIG. 6: (Color online) The stability (E) of UO_{2+x}, NpO_{2+x} and PuO_{2+x}, measured relative to AnO_2 and O_2 (oxidation energy). The numbers represent the most stable configuration for each composition. We have also included hydrogen-containing compounds. Phase separation follows if the oxidation energies exhibit negative curvature. For example this is evidently the case for UO_{2+x} and since the U_4O_9 compound has the most negative oxidation energy the low temperature equilibrium must involve UO_2-U_4O_9.

and U_4O_9(bccr), the {111} in-plane patterns of split di-interstitials are similar to the ordering of triangular oxygen clusters that was obtained by Campbell and Ellis from LEED measurements of the surface structure in oxidized UO_2[52,53], thus supporting the pivotal role of the split di/quad-interstitial as the fundamental building block in UO_{2+x}. Some discrepancies still exist between the patterns in Fig. 5 and Refs. 52,53, above all the detailed ordering pattern in Refs. 52,53 is unclear, which,

in our model, would translate into uncertainties regarding the ordering of split quad-interstitials.

The U_4O_9 structures based on cubo-octahedron clusters within the $2 \times 2 \times 2$ cell are not as stable as U_4O_9(bcc)/U_4O_9(bccr). The U_4O_9(Cubo) oxidation energy is -2.13 eV compared to -2.57 eV for U_4O_9(bccr). This contradicts the established experimental U_4O_9 structure model[10,11], which favors an ordering pattern based on cubo-octahedrons, as an alternative we propose that the low-temperature U_4O_9 compound constitutes an ordered array of split quad/di-interstitial clusters, possibly arranged as in the U_4O_9(bccr) model compound.

The experimental oxidation energy for U_4O_9 is ≈ -1.8 eV[54], which is notably higher (less negative) than the calculated value of -2.57 eV for U_4O_9(bccr). This discrepancy may be partially due to uncertainties in the choice of the Hubbard U parameter and/or the exchange-correlation potential. Test calculations using GGA+U with $U = 3.5$ and $J = 0.35$ eV give an oxidation energy of -1.94 eV for U_4O_9(bccr), which agrees better with experiments. The GGA+U UO_2 lattice parameter is overestimated by 0.06 Å and the bulk modulus is predicted to be 194 GPa, in good agreement with experiments (see Table II). The relative stabilities of U_4O_9 compounds within GGA+U are U_4O_9(Oct.) (-0.79 eV), U_4O_9(111) (-1.47 eV), U_4O_9(1-10) (-1.63 eV), U_4O_9(bcc) (-1.90 eV) and U_4O_9(bccr) (-1.94 eV), which is the same stability sequence as obtained for LDA+U and even the stability differences are rather similar (U_4O_9(Oct.) deviates slightly from this conclusion). From this we conclude that even though the current LDA+U functional overestimates the oxidation energy of UO_{2+x} by 0.6-0.7 eV, this shift seems to be rather constant and, most importantly, this implies that the relative defect stabilities, and thus also the proposed ordering patterns, should be reliable.

In UO_2 there is a single U-O distance of 2.36 Å (for the calculated lattice constant), but oxidation of UO_2 creates a distribution of U-O bond lengths. For U_4O_9(Oct.), the calculations predict the nearest neighbor U-O bond length to be 2.20 Å and this is largely achieved by displacing the fluorite oxygen ions while the uranium sublattice remains essentially intact. For the split di-interstitial U_4O_9 compounds there is obviously a significant displacement of the oxygen sublattice, but, unlike the U_4O_9(Oct.) compound, there is also an accompanying distortion of the uranium sublattice. Fig. 7 illustrates these properties in terms of the uranium radial distribution function for U_4O_9(Oct.) and U_4O_9(bccr). Similar arguments also hold for point defects based on octahedral interstitials and split di-interstitials. EXAFS measurements by Conradson *et al.* have provided new information about the local structure in UO_{2+x} compounds[32]. Most notably they predict very short oxo-type of U-O bonds (1.74 Å)[32]. Fig. 7 compares the radial distribution function, g(r), from the U_4O_9 structure models that are used in the present work with g(r) derived from EXAFS measurements[32]. Qualitatively, the U_4O_9(bccr) structure model reproduces the broad distribution of U-O bonds between 2.15 and 2.75 Å. The short U-O (2.1-2.2 Å) distances obtained from the structure models proposed here uniquely originate from U^{5+}-O^{2-} distances. The oxo-bonds at 1.7-1.8 Å in the EXAFS data are not present in any of the calculated distribution functions, which suggests that the oxo-type of bonds should originate from domains, interfaces or surfaces where the regular fluorite structure breaks down.

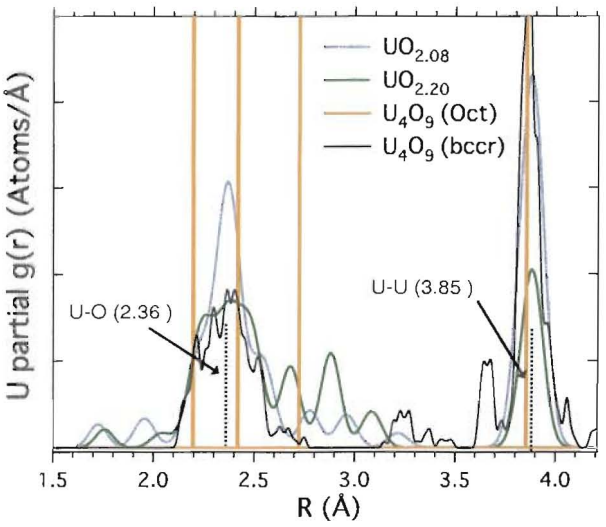

FIG. 7: (Color online) The uranium partial radial distribution function, g(r), calculated from U_4O_9(bccr) and U_4O_9(Oct.) and compared to g(r) from EXAFS measurements on two different UO_{2+x} samples[32]. The U-O and U-U labels (dotted vertical lines) indicate the bond distances in UO_2.

2. *Neptunium and Plutonium dioxides*

The ordering patterns established above for U_4O_9 have also been applied to the neptunium and plutonium based oxides. The corresponding stabilities are collected in Table II. Np_4O_9 exhibits almost the same sequence of ordered compounds as U_4O_9, though overall the oxidation energy increases significantly and the Np_4O_9(Oct.) structure is even unstable. However, its stability can be increased considerably (0.76 eV) by allowing half of the octahedral interstitials to form molecular O_2 species with regular fluorite oxygen ions (further discussed for Pu_4O_9). The relative stability of Np_4O_9(bcc) and Np_4O_9(bccr) is shifted between the U and Np based dioxides. For Np_4O_9 the two structures are almost degenerate. As pointed out for NpO_{2+x}, the high oxidation energy for Np_4O_9 compared to U_4O_9 is a consequence of the smaller gain in O-2p band energy relative the An-5f delocalization energy, which in turn is due to the decreased separation of An-5f and O-2p orbitals in NpO_2 compared to UO_2. In order to verify that the decreased stability of Np_4O_9 is principally a band structure effect and not due to the smaller volume of NpO_2 com-

pared to UO_2, we calculated the NpO_2 oxidation thermodynamics at the UO_2 lattice constant without finding any significant changes. The charge transfer in NpO_{2+x} benefits from high degree of hybridization to a larger extent than for UO_{2+x}, which is the reason why NpO_{2+x} and Np_4O_9 exhibit an even stronger preference for split di-interstitial type of structures than UO_{2+x} compounds. NpO_{2+x} reveals a similar two-phase field as UO_{2+x} (see Fig. 6); the increased negative curvature of the stability suggests that the disordering temperature may be even higher than for UO_{2+x}. Though, in this context we recall that according to the experimental phase diagram NpO_{2+x} is unstable or possibly meta-stable with respect to NpO_2+Np_2O_5[14,15] or NpO_2+O_2[5,14,15]. According to Ref. 15 the Np_2O_5 oxidation energy is -0.15 eV, which, in relation to our calculated data, implies that Np_4O_9 could exist as a stable compound. However, from U_4O_9 we also know that the LDA+U calculations tend to overestimate the stability of oxidation products. If this overestimation is of the same order of magnitude for Np_4O_9 as for U_4O_9 (0.6-0.7 eV), the stability of Np_4O_9 is almost identical to Np_2O_5. In both cases the oxidation energy is close to 0 eV, implying that disassociation into NpO_2+O_2 should take place already at moderate temperatures and for small changes in the oxygen chemical potential. These conclusions qualitatively agree with the experimental analyses by Neck *at al.*[5] and they are also consistent with the difficulty of preparing NpO_{2+x} by direct oxidation of NpO_2[14]. Moreover, since the oxidation energies of Np_4O_9 and Np_2O_5 are not very different, the fluorite based NpO_{2+x} phase can probably be stabilized by the addition of uranium.

Table II demonstrates that the properties of the Pu_4O_9 compounds are quite different from the corresponding uranium and neptunium compounds. Pu_4O_9(1-10) is the structure of highest energy (this structure is low in energy for U_4O_9 and Np_4O_9) and $Pu_4O_9(111_0)$ is one of the most stable structures (this structure is high in energy for U_4O_9 and Np_4O_9). Pu_4O_9(bcc) is the most stable compound. There is also an octahedral interstitial structure that is almost as stable as Pu_4O_9(bcc), but this Pu_4O_9 structure includes an O_2 molecular species that is created from an octahedral interstitial oxygen ion and one of its nearest neighbor regular fluorite oxygen ion. The O-O bond distance for this molecular species is 1.43 Å. In our calculations, the O_2 species constitute half of the interstitials and the other half acts as regular octahedral interstitials. There is minimal charge transfer from plutonium ions to the O_2 species, which makes it an uncharged molecule rather than an O_2^- or O_2^{2-} ion. The formation of O_2 species lowers the energy by 0.46 eV compared to regular octahedral interstitials. The oxidation energy for Pu_4O_9 is just below zero and PuO_2 should consequently be rather difficult to oxidize. This seems to correlate with its unique structural properties. We have already concluded that the instability of PuO_{2+x} follows from the fact that in PuO_2 the 5f orbitals completely overlap with the O-2p band, implying that the Pu-5f to excess O-2p charge transfer does not result in any significant gain in band energy, even if maximum hybridization is assumed. Consequently, charge transfer must be more difficult and this explains why the excess oxygen ions are not able to attract two full electrons from the plutonium ions, or more precisely attain the O^{2-} valence state (see Sec. III A). Analogous arguments partially hold for NpO_{2+x}, but since the Np-5f states are situated at the top of the O-2p band charge transfer is still easier than for PuO_{2+x}. The incomplete charge transfer in PuO_{2+x} (and NpO_{2+x}) creates a hole in the O-2p band (see Fig. 8), which from a chemical point of view is unfavorable. The formation of O_2 species within the lattice in part removes the O-2p hole and separates the remaining states from the valence band, thus explaining the increased stability for this compound. The most stable Pu_4O_9(bcc) compound exhibits a high degree of hybridization and thus also yields high plutonium to excess oxygen charge transfer (i.e. valence states of Pu^{5+} and O^{2-}). There are still O-2p hole states for Pu_4O_9(bcc) but they are located within the band gap. At the same time the repulsive Coulomb contribution is more efficiently handled for Pu_4O_9(bcc) than for, e.g., Pu_4O_9(1-10). Our calculations show that the relative stabilities of PuO_{2+x} structures are correlated with the ability to separate the O-2p hole states from the valence band and move them into either the band gap or the conduction band. This conclusion is similar to the observation that the energy of Pu_4O_9(Oct.) decreases by displacing the octahedral interstitial from its high symmetry position made by Prodan *et al.*[22].

D. Hydrogen affinity of AnO_{2+x} and An_4O_9

The PuO_2 oxidation thermodynamics presented in the previous section partially contradict the findings by Haschke *et al.*[7,8], who claimed to be able to oxidize PuO_{2+x} up to x=0.27. On the other hand our results support failures to produce bulk PuO_{2+x} from PuO_2 by using pure oxygen as oxidation agent[5,6]. The fact that Haschke *et al.* used moist air as oxidation agent and the fact that Conradson *et al.*[13] found PuO_{2+x} to readily incorporate H_2O or its radiolysis products (e.g. OH^-) in the lattice point to the critical role of these species in the oxidation process. Neck *et al.*[5] further emphasized the importance of H_2O by, based on analogies to UO_{2+x}, estimating anhydrous PuO_{2+x} to be unstable, which disagrees with the oxidation mechanism proposed by Haschke *et al.*[7,8]. Their estimated Pu_4O_9 oxidation energy of 0.13 eV[5] is higher than the present calculations (-0.14 eV), though from U_4O_9 we know that the LDA+U calculations have a tendency to predict too negative oxidation energies. Assuming the Pu_4O_9 error to be similar to U_4O_9, e.g. 0.6-0.7 eV, we predict even more positive oxidation energies than Neck *et al.*[5], thus emphasizing the endothermic character of this reaction. On the other hand Neck *et al.* predicted hydrous Pu_4O_9 (Pu_4O_9 associated with H_2O) to have slightly negative oxidation

energy (-0.12 eV)[5]. These observations motivate us to study oxidation thermodynamics based on absorption of OH^- or H_2O in the AnO_2 lattice. This was achieved by inserting hydrogen atoms into the $2\times2\times2$ supercell that contains a single oxygen interstitial. The hydrogen atoms prefer to bind to the oxygen ion in the octahedral interstitial position and align themselves in (111) directions, which means that they are situated in-between two oxygen ions but the distance to the octahedral oxygen ion is shorter than to the regular fluorite ion. In the case of H_2O the two hydrogen atoms form an approximately 180° angle with the interstitial oxygen ion. Using similar procedures as for the $2\times2\times2$ cell we have also studied $An_4O_8(OH)_2$ within the same cell as was used for An_4O_9(111). The oxidation energies are summarized in Table II and they are also illustrated in Fig. 6. For PuO_{2+x} the presence of OH^- species lowers the oxidation energy significantly, in particular for $Pu_4O_8(OH)_2$, so that oxidation of PuO_2 becomes an exothermic reaction. The difference in oxidation energy between the OH^- point defect in the $2\times2\times2$ supercell and $Pu_4O_8(OH)_2$ indicates that there is a tendency to phase separate into PuO_2 and $Pu_4O_8(OH)_2$ domains. Measured against oxidation based on OH^- species, absorption of H_2O species is less likely to occur; as an example the oxidation energy of $PuO_2(H_2O)_{\frac{1}{32}}$ is 0.48 eV. Our results suggest that oxidation of PuO_2 requires the presence of H_2O and its radiolysis products in order to take place at any significant rate. This would explain why Gouder *et al.*[56] failed to oxidize PuO_2 using pure oxygen as oxidation agent, while Haschke *et al.* observed oxidation in moist air. The lattice constant of $Pu_4O_8(OH)_2$ exhibits a small expansion, which agrees with the experimental observation by Haschke *et al.*[7]. In this context we observe that U_4O_9(1-10) and Np_4O_9(1-10) both contract by 0.01-0.02 Å, which again emphasizes the distinctive properties of PuO_{2+x}. Experimentally, U_4O_9 contracts by 0.03 Å, measured as an average for the $4\times4\times4$ unit cell[10]. The reason for $Pu_4O_8(OH)_2$ being the most stable oxidation product of PuO_2 lies in the change of the band structure induced by hydrogen. Fig. 8 illustrates how the orbitals of the OH^- species are situated about 0.50 eV below the main O-2p band, which implies that the electron transferred from plutonium to the OH^- species moves down from the hybrydized O-2p–Pu-5f band to the OH band and this results in a gain in the band energy, much like the process for split di-interstitials in UO_{2+x}. Also, the electron donated by hydrogen means that only one plutonium electron needs to be transferred to achieve a filled O-2p orbitals. In this context we recall that, due to the overlap of the Pu-5f orbitals with the O-2p band, charge transfer to the excess O-2p orbitals in PuO_{2+x} is incomplete and oxidation is unfavorable. The negative oxidation energies of $Pu_4O_8(OH)_2$ and $PuO_2(OH)_{1/32}$ are consistent with the oxidation energy of -0.12 eV predicted by Neck *et al.* for hydrous PuO_2. Our experience from U_4O_9 indicate that we slightly overestimate the stability of oxidation products and, consequently, we expect the oxidation energy of $Pu_4O_8(OH)_2$ to increase (become less negative), however even if the upper limit of the error for U_4O_9 is applied as correction (0.7 eV) the oxidation energy of $Pu_4O_8(OH)_2$ stays (slightly) negative.

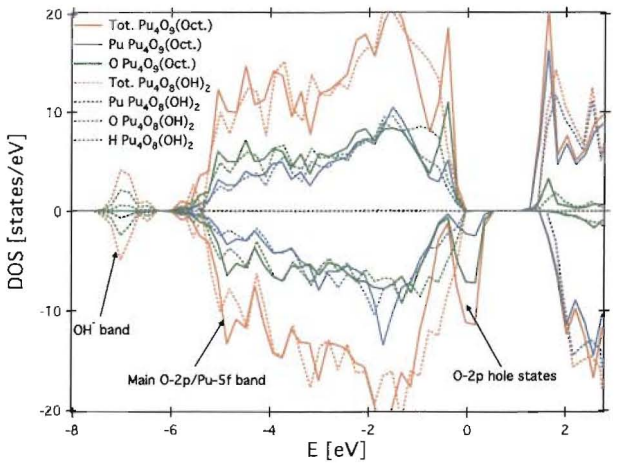

FIG. 8: (Color online) Densitiy of states (DOS) and projected density of states (PDOS) for Pu_4O_9 with octahedral interstitials (Pu_4O_9(Oct.)) and $Pu_4O_8(OH)_2$. For the Pu_4O_9(Oct.) structure we observe the O-2p hole states at the top of the valence band. By introducing certain distortions to the octahedral Pu_4O_9 structure, the O-2p hole states may separate from the valence band and occupy position in the band gap, which is a process that lowers the energy. The unoccupied O-2p states at the top of the valence band disappear for $Pu_4O_8(OH)_2$ and instead the OH^- band appears below the main O-2p band. The highest occupied state is at 0 eV.

Even though the $UO_2(OH)_{\frac{1}{32}}$ and $U_4O_8(OH)_2$ compounds have negative oxidation energies, both are less stable than the corresponding pure oxides and thus they release any absorbed hydrogen, which agrees with established oxidation thermodynamics of UO_2[4]. $U_4O_8(OH)_2$ exhibits a similar OH^- band below the main O-2p band as $Pu_4O_8(OH)_2$. The fact that UO_{2+x} does not attract hydrogen means that the contribution from decreased band energy due to O-2p hybridization is more important. Notice that $U_4O_8(OH)_2$ is indeed more stable than the U_4O_9(Oct.) structure, for which hybridization effects are small compared to the most stable U_4O_9 compounds. The $Np_4O_8(OH)_2$ compound is slightly more stable than Np_4O_9(bcc). In qualitative agreement with this observation, Neck *et al.* estimated the oxidation energy of hydrous NpO_2 to be negative, and thus somewhat lower than for anhydrous NpO_2[5].

IV. CONCLUSIONS

The excess oxygen ions in hyperstoichiometric actinide dioxides, AnO_{2+x} (An = U, Np or Pu), tend to form clusters of interstitial oxygen ions and, using density functional theory calculations, we have established the so-called split di-interstitial, illustrated in Fig. 1, as

the fundamental building block of these defect clusters. The most stable configuration constitutes two split di-interstitials that are rotated 180° with respect to each other, as illustrated in Fig. 4. Our calculations demonstrate that the stability of these clusters is an effect of the increased hybridization between actinide ions and excess oxygen ions that is enabled by their particular geometry. This hybridization competes with Coulomb repulsion among the An^{5+} ions and among the O^{2-} ions, which is a contribution that favors structures based on regular octahedral interstitials, and the emergence of the UO_2+U_4O_9 two-phase field is a manifestation of optimizing this balance. Moreover, we predict a new ground-state structure for U_4O_9 that is based on a superstructure of split quad-interstitials, which, alternatively, can be visualized as a stacking of {111} planes that contain an ordered arrangement of split di-interstitials.

Knowledge about the clustering patterns of excess oxygen ions in AnO_{2+x} is prerequisite for accurately assessing, e.g., thermodynamic properties and the insights acquired from the present density functional theory calculations thus allow us to model the oxidation thermodynamics of UO_2, NpO_2 and PuO_2 within fluorite derived structures. UO_2 exhibits strongly negative oxidation energy and reacts readily with oxygen, while NpO_2 is significantly harder to oxidize and PuO_2 is predicted to have positive, or just slightly negative, oxidation energy. The degree of AnO_2 oxidation is a function of the position of the An-5f electrons relative the O-2p band. If these states are situated above the O-2p band, oxidation easily occurs (UO_2), while the overlap of An-5f and O-2p states in PuO_2 surpresses oxidation. Hydrolysis products are able to offset this effect and turn oxidation of PuO_2 into an exothermic process, which is a very important observation since it explains recent uncertainties regarding the stability of PuO_2 oxidation products. Both NpO_{2+x} and PuO_{2+x} have a high affinity for hydrogen, especially compared to UO_{2+x}. Following the trends for the position of the 5f electrons along the actinide series we expect that actinide dioxides to the left of UO_2 (PaO_2) should oxidize easily, while actinide oxides to the right of PuO_2 should be very hard to oxidize.

V. ACKNOWLEDGEMENTS

Work at Los Alamos National Laboratory was funded by the Global Nuclear Energy Partnership Fuels Campaign, and OBES Division of Chemical Sciences under contract W-7405. D.A.A. also acknowledges support from the Seaborg Institiute. Los Alamos National Laboratory is operated by Los Alamos National Security, LLC, for the National Nuclear Security Administration of the U.S. DOE under contract DE-AC52-06NA25396.

[1] Y. S. Kim, J. Nucl. Mater. **279**, 173 (2000).
[2] L. R. Morss in The Chemistry of the Actinide Elements 2nd edn Vol. 2 (eds. J. J. Katz, G. T. Seaborg and L. R. Morss) 1278-1360 (Chapman and Hall, London, 1986).
[3] M. W. Chase, *et al.* JANAF Thermochemical Tables 3rd edn Part II Cr-Zr, 927-1856 (AIP, New York, 1985).
[4] I. Barin, O. Knacke and O. Kubaschewski, Thermochemical Properties of Inorganic Substances. (suppl.) 1-861 (Springer, Berlin, 1977).
[5] V. Neck, M. Altmaier, Th. Fanghänel, J. Alloys and Compounds **444-445**, 464 (2007).
[6] C. Keller in Comprehensive Inorganic Chemistry Vol. 5 Actinides (eds. J. C. Bailar, H. J. Emeleus, R. Nyholm, and A. F. Trotman-Dickenson) 219-276 (Pergamon, Oxford, 1973).
[7] J. M. Haschke, T. H. Allen and L. A. Morales, Science **287**, 285 (2000).
[8] J. M. Haschke and T. H. Allen, J. Alloys Compd. **336**, 124 (2002).
[9] P. Martin, S. Grandjean, M. Ripert, M. Freyss, P. Blanc and T. Petit, J. Nucl. Mater. **320**, 138 (2003).
[10] D. J. M. Bevan, I. E. Grey and B. T. M. Willis, J. Solid State Chem. **61**, 1 (1986).
[11] R. I. Cooper and B. T. M. Willis, Acta Cryst. **A60**, 322 (2004).
[12] S. D. Conradson, B. D. Begg, D. L. Clark, C. Den Auwer, F. J. Espinosa- Faller, P. L. Gordon, N. J. Hess, R. Hess, D. W. Keogh, L. A. Morales, M. P. Neu, W. Runde, C. D. Tait, D. K. Veirs and P. M. Villella, Inorg. Chem. **42**, 3715 (2003).
[13] S. D. Conradson, B. D. Begg, D. L. Clark, C. den Auwer, M. Ding, P. K. Dorhout, F. J. Espinosa-Faller, P. L. Gordon, R. G. Haire and N. J. Hess, J. Am. Chem. Soc. **126**, 13443 (2004).
[14] K. Richter, C. Sari, J. Nucl. Mater. **148**, 266 (1987).
[15] Chemical Thermodynamics of Neptunium and Plutonium, Vol. 4 (eds. R. J. Lemire, J. Fuger, H. Nitsche, P. Potter, M. H. Rand, J. Rydberg, K. Spahiu, J. C. Sullivan, W. J. Ullman, P. Vitorge and H. Wanner), North-Holland, Amsterdam, 2001.
[16] M. Freyss, T. Petit, J.-P. Crocombette, J. Nucl. Mater. **347**, 44 (2005).
[17] P. A. Korzhavyi, L. Vitos, D. A. Andersson and B. Johansson, Nature Materials **3**, 225 (2004).
[18] J. P. Crocombette, F. Jollet, L. T. Nga and T. Petit, Phys. Rev. B **64**, 104107 (2001).
[19] M. Iwasawa, Y. Chen, Y. Kaneta, T. Ohnuma, H. Y. Geng and M. Kinoshita, Mater. Trans. **47**, 2651 (2006).
[20] F. Gupta, G. Brillant and A. Pasturel, Phil. Mag. **87**, 2561 (2007).
[21] H. Y. Geng, Y. Chen, Y. Kaneta and M. Kinoshita, Phys. Rev. B **75**, 054111 (2007).
[22] I. D. Prodan, G. E. Scuseria, J. A. Sordo, K. N. Kudin and R. L. Martin, J. Chem. Phys. **123**, 014703 (2005).
[23] L. Petit, A. Svane, Z. Szotek, W. M. Temmerman, Science **301**, 498 (2003).
[24] S. L. Dudarev, D. N. Manh and A. P. Sutton, Phil. Mag. B **75**, 613 (1997).

[25] B. Sun, P. Zhang and X.-G Zhao, J. Chem. Phys. 128, 084705 (2008).
[26] B. Sun and P Zhang, Chinese Physics B **17**, 1364 (2008).
[27] R. Laskowski, G. K. H. Madsen, P. Blaha and K. Schwarz, Phys. Rev. B **69**, 140408 (2004).
[28] I. D. Prodan, G. E. Scuseria, R. L. Martin, Phys. Rev. B **76**, 033101 (2007).
[29] K. N. Kudin, G. E. Scuseria, and R. L. Martin, Phys. Rev. Lett. **89**, 266402 (2002).
[30] I. D. Prodan, G. E. Scuseria and R. L. Martin, Phys. Rev. B **73**, 45104 (2006).
[31] Q. Y. and S. Y. Savrasov, Phys. Rev. Lett. **100**, 225504 (2008).
[32] S. D. Conradson, D. Manara, F. Wastin, D. L. Clark, G. H. Lander, L. A. Morales, J. Rebizant and V. V. Rondinella, Inorg. Chem. **43**, 6922 (2004).
[33] B. T. M. Willis, J. Chem. Soc., Faraday Trans., **83**, 1073 (1987).
[34] B. T. M. Willis, Proc. Br. Ceram. Soc., 1964, 1, 9; Acta Crystallogr., Sect A **34**, 88 (1978).
[35] B. T. M. Willis, Nature **197**, 755 (1963).
[36] G. Kresse and J. Hafner, Phys. Rev. B **48**, 13115 (1993).
[37] G. Kresse and J. Furthmüller, Comp. Mater. Sci. **6**, 15 (1996).
[38] G. Kresse and J. Furthmüller, Phys. Rev. B **54**, 11169 (1996).
[39] G. Kresse and D. Joubert, Phys. Rev. B **59**, 1758 (1999).
[40] P. E. Blöchl, Phys. Rev. B **50**, 17953 (1994).
[41] A. I. Liechtenstein, V. I. Anisimov and J. Zaanen, Phys. Rev. B **52**, R5467 (1995).
[42] H. J. Monkhorst and J. D. Pack, Phys. Rev. B **13**, 5188 (1976).
[43] S. Kurth, J. P. Perdew and P. Blaha, Int. J. Quantum Chem. **75**, 889 (1999).
[44] D. A. Andersson, S. I. Simak, B. Johansson, I. A. Abrikosov and N. V. Skorodumova, Phys. Rev. B **75**, 035109 (2007).
[45] A. D. Murray and B. T. M. Willis, J. Solid State Chem. **84**, 52 (1990).
[46] D. A. Andersson, C. Deo and B. P. Uberuaga, in preparation.
[47] T. Ichinomiya, et. al., in preparation.
[48] K. Govers, S. Lemehov, M. Hou, and M. Verwerft, J. Nucl. Mater. **366**, 161 (2007).
[49] C. Allen, P. A. Tempest, J. W. Tyler, Nature **295**, 48 (1982).
[50] Sickafus *et al*, Los Alamos Series Report No. LA-14205, 2006.
[51] F. Garrido, L. Nowicki and L. Thome, Phys. Rev. B **74**, 184114 (2006).
[52] B. D. Campbell and W. P. Ellis, Surf. Sci. **68**, 469 (1977).
[53] G. C. Allen and P. A. Tempest, Proc. Roy. Soc. Lon. A **406**, 325 (1986).
[54] P.-Y. Chevalier, E. Fisher and B. Cheynet, J. Nucl. Mater. **303**, 1 (2002).
[55] V. A. Kurepin, J. Nucl. Mater. **303**, 65 (2002).
[56] T. Gouder, A. Seibert, L. Havela and J. Rebizant, Surf. Sci. **601**, L77 (2007).
[57] T. Yamashita, N. Nitani, T. Tsuji, H. Inagaki, J. Nucl. Mater. **247**, 90 (1997).
[58] U. Benedict, S. Dabos, C. Dufour and J. C. Spirlet, J. Less Common Metals **121**, 461 (1986).
[59] M. Idiri, T. Le Bihan, S. Heathman and J. Rebizant, Phys. Rev. B **70**, 014113 (2004).
[60] K. Naito, J. Nucl. Mater. **51**, 126 (1974).